




## Article

# Electrochemical and Optical Properties of Fluorine Doped Tin Oxide Modified by ZnO Nanorods and Polydopamine

Roman Viter<sup>1,2,\*</sup>, Viktoriia Fedorenko<sup>1</sup>, Inga Gabriunaite<sup>3</sup>, Irina Tepliakova<sup>1</sup>, Simonas Ramanavicius<sup>1,3</sup>, Viktoriia Holubnycha<sup>4</sup>, Arunas Ramanavicius<sup>3</sup> and Aušra Valiūnienė<sup>3,\*</sup>

<sup>1</sup> Institute of Atomic Physics and Spectroscopy, University of Latvia, 19 Raina Blvd., LV-1586 Riga, Latvia  
<sup>2</sup> Center for Collective Use of Scientific Equipment, Sumy State University, 31, Sanatornaya St., 40018 Sumy, Ukraine  
<sup>3</sup> Faculty of Chemistry and Geosciences, Institute of Chemistry, Vilnius University, Naugarduko Str. 24, LT-03225 Vilnius, Lithuania  
<sup>4</sup> Medical Institute Sumy State University, Sanatorna Str. 1, 40007 Sumy, Ukraine  
\* Correspondence: roman.viter@lu.lv (R.V.); ausra.valiuniene@chf.vu.lt (A.V.)

**Abstract:** Abstract Various forms of zinc oxide (ZnO) are frequently used in the design of optical and electrochemical sensors. However, the optical and electrochemical properties of ZnO should be properly adjusted depending on the application area. Therefore, in this work, we have investigated changing/tuning the properties of ZnO by depositing a layer of polydopamine (PDA) on its surface. In order to perform this investigation, the surface of fluorine-doped tin oxide (FTO) was modified with the layer of ZnO nanorods and PDA. ZnO nanorods were synthesized by hydrothermal synthesis technique, and after the synthesis, they were coated with polydopamine exploiting the self-polymerization of dopamine. The nanostructures were investigated by using electrochemical and optical methods. Electrochemical impedance spectroscopy measurements showed that electrochemical properties of FTO-ZnO and FTO-ZnO-PDA nanostructures could be changed by the variation of both—applied electrical potential and/or exposition towards lighting. Interaction between ZnO-PDA and bovine serum albumin (BSA) molecules has been investigated by (photo)electrochemical and photoluminescence methods. A mechanism of possible interaction between BSA and the ZnO-PDA surface has been proposed.

**Keywords:** polydopamine (PDA); photoluminescence; cyclic voltammetry; electrochemical impedance spectroscopy (EIS); self-polymerization; zinc oxide (ZnO) nanorods; fluorine doped tin oxide (FTO)



**Citation:** Viter, R.; Fedorenko, V.; Gabriunaite, I.; Tepliakova, I.; Ramanavicius, S.; Holubnycha, V.; Ramanavicius, A.; Valiūnienė, A. Electrochemical and Optical Properties of Fluorine Doped Tin Oxide Modified by ZnO Nanorods and Polydopamine. *Chemosensors* **2023**, *11*, 106. <https://doi.org/10.3390/chemosensors11020106>

Academic Editor: Manel del Valle

Received: 13 November 2022

Revised: 24 January 2023

Accepted: 27 January 2023

Published: 2 February 2023



**Copyright:** © 2023 by the authors. Licensee MDPI, Basel, Switzerland. This article is an open access article distributed under the terms and conditions of the Creative Commons Attribution (CC BY) license (<https://creativecommons.org/licenses/by/4.0/>).

## 1. Introduction

Core-shell inorganic-organic composite nanomaterials belong to a new class of materials with advanced optical, electrical, electrochemical and sensing properties [1]. Some of these materials demonstrate advanced optical signals, new photoluminescence peaks (PL) and good biocompatibility [2]. Core-shell structures consist of an innercore and an outershell, both consisting of different materials [3–5]. They are widely applied in such fields as drug delivery [6], sensors [7], catalytic evolution of hydrogen [8], wastewater treatment, reduction of organic dyes [9,10], or photocatalysis under both UV and visible range illumination [11,12]. Among different nanomaterials, a combination of ZnO and polydopamine (PDA) shows good prospects for biomedical [13] and sensing or biosensing applications [14]. The deposition of self-polymerized conformal coating of PDA nanolayer on ZnO nanorods was reported [2,14]. ZnO-PDA structural properties have been investigated by using X-ray diffraction (XRD), Raman and transmission electron microscope (TEM). TEM investigations showed conformal coating of ZnO by PDA. The PDA layer thickness increases from 6 nm to 10 nm with an increase in dopamine concentration during polymerization. Comparative analysis of XRD spectra of ZnO before and after PDA deposition showed that the intensity of ZnO XRD peaks decreased after PDA layer deposition.

Raman spectra after PDA deposition showed new peaks related to C=C, C-C and C-N vibrations in the PDA structure.

A study of the optical properties of ZnO-PDA nanostructures showed an increase of absorbance in the UV-Vis region and a red shift of band gap in ZnO-PDA nanostructures. Photoluminescence of ZnO-PDA nanostructures is significantly quenched compared to deposited ZnO. It was assumed that the PDA layer formed on ZnO nanorods resulted in photoluminescence quenching and the shift of photoluminescence peak positions [15].

A mechanism of interaction between ZnO and PDA and ZnO/PDA interface forming was proposed. Defect states on the ZnO surface (oxygen vacancies) have formed chemical bonds with hydroxyl groups in the PDA molecule. The proposed model of ZnO-PDA layer formation suggested the involvement of ZnO structural defects (oxygen/zinc vacancies) in the formed PDA layer [2]. PDA concentration was one of the key parameters which can be applied for the tailoring of optical ZnO-PDA nanocomposite properties [15]. It was shown that the shift of PL and the decrease of the optical band gap in ZnO-PDA nanocomposites were proportional to PDA concentration [15]. The negative surface charge of ZnO-PDA was proved by zeta potential measurement, and the electrostatic interaction of ZnO-PDA with positively charged poly-L-lysine (PLL) was applied for sensor design. Electrostatic interaction of ZnO-PDA with PLL induced significant changes in the photoluminescence spectra of the samples, e.g., PL intensity decreased in the UV region for all ZnO-PDA samples after the interaction with PLL. However, changes in PL spectra in the visible range of wavelengths were observed only for low concentrations of PDA [15]. The interaction between ZnO-PDA nanostructures with biomolecules showed that mechanisms of interaction are tailored by the properties of the ZnO-PDA interface. However, for a wider application of ZnO-PDA core-shell structures, a deeper understanding of processes happening on the surface and ZnO-PDA-interphase is required. The combination of photo- and electrochemical methods enables to advance of the analysis of charge transfer properties between different components of composite nanostructures [16]. Therefore, the analysis based on photoelectrochemical spectroscopy, cyclic voltammetry (CV), amperometry and electrochemical impedance spectroscopy (EIS) data is useful in the prediction of charge transfer mechanisms at such complex interfaces [14,17].

Electrochemical impedance spectroscopy is a very useful technique to investigate electrical properties of high-resistance materials because the impedance is measured in alternating current, in opposite to conventional electrochemical techniques (voltammetry, amperometry), which involve direct current (DC) at an electrode as a function of applied voltage. By means of EIS, we can avoid possible changes on the electrode surface and obtain quantitative data. EIS method is a universal technique to analyze various electrochemical systems, such as batteries [18–20], biosensors [17,21–24], solar cells [25–27], corrosion tests [28–30], and capacitors [31–33]. The main advantage of alternating current-based impedance measurements is that the conditions of the experiment do not exceed steady-state conditions; thus, even sensitive or reactive samples can be investigated by EIS. Additionally, the obtained impedance spectra measured over a wide range of alternating current frequencies (from a few mHz to several kHz) can be fitted with results calculated using an equivalent circuit model, and various kinetic parameters (e.g., charge transfer resistance ( $R_{ct}$ ), Warburg impedance ( $W$ ), etc.) can be determined for various electrochemical systems [34].

Various forms of zinc oxide are frequently used in the design of optical and electrochemical sensors. However, the optical and electrochemical properties of ZnO should be properly adjusted depending on the application area. Therefore, in this work, we have investigated changing/tuning the properties of ZnO by depositing the polydopamine layer. We have performed an assessment of FTO-ZnO-PDA nanostructures by the assessment of photoluminescence, cyclic voltammetry, chronoamperometry and electrochemical impedance spectroscopy. By using (photo)electrochemical and photoluminescence methods, the interaction between ZnO-PDA and bovine serum albumin (BSA) molecules has

been investigated, and the mechanism of possible interaction between BSA and ZnO-PDA surface has been proposed in this research as well.

## 2. Materials and Methods

### 2.1. Materials

Zinc acetate dehydrates, hexamethylenetetramine, 2-propanol (IPA), ethanolamine, sodium sulphate, zinc nitrate hexahydrate, dopamine hydrochloride 99%, phosphate buffered saline (tablet) were purchased from Sigma Aldrich (Riga, Latvia). Glutaraldehyde 25% was ordered from Carl Roth (Karlsruhe, Germany). Tris(hydroxymethyl)aminomethane 99% was purchased from Alfa Aesar and was used without further purification.

The FTO-glass substrates (19 mm × 12 mm) were cleaned by successive sonication with deionized water and ethanol, with drying before final use. Oxygen plasma treatment for 15 min was performed to remove organic contaminations. After the mentioned cleaning pretreatment, the ZnO-PDA nanocomposite was deposited on the FTO-coated glass surface.

### 2.2. Fabrication of ZnO-PDA Nanostructures

ZnO nanorods (ZnO-NRs) were deposited on conducting FTO glass by a hydrothermal method, as described in some of our previous references [35,36], followed by PDA deposition [2]. Briefly, zinc acetate in methanol solution (5 mM) was deposited on the FTO glass substrate by drop-casting technique. After, the annealing at 350 °C for 1 h was performed to transform zinc acetate into zinc oxide. Then, hydrothermal growth of ZnO-NRs was performed by immersing the substrates with a zinc seed layer in an aqueous solution of zinc nitrate (50 mM) and hexamethylenetetramine (50 mM) at 95 °C for 4 h. After the ZnO-NRs growth, the samples were washed with H<sub>2</sub>O and dried at room temperature.

PDA was deposited on FTO glass covered with ZnO-NRs by self-polymerization of dopamine in an alkaline buffer solution (TRIS buffer, 10 mM, pH 8.5) for 2 h [2]. The concentration of dopamine in the solution varied from 0.3 to 0.7 mg/mL. Prior to further study, the samples were washed with H<sub>2</sub>O and dried. Three independently prepared samples have been investigated during this research, and average results are presented in this study.

### 2.3. Assessment of Structure and Electronic Properties of ZnO-PDA Nanostructures

The structural properties of the ZnO-PDA nanostructures were studied by scanning electron microscopy (SEM) (Zeiss Evo HD15 SEM from Zeiss Ltd. (Jena, Germany)). Attenuated total reflectance Fourier-transform infrared spectroscopy (ATR-FTIR) spectrometer Alfa II from Bruker Optics (Bremen, Germany) was used to study forming of the ZnO-PDA composites in the range of 1000–4000 cm<sup>-1</sup>. The background of the FTIR spectra was subtracted automatically at the end of the measurement.

### 2.4. Evaluation of Optical and Electrochemical Properties of ZnO-PDA Nanostructures

Electrochemical measurements were performed in a hand-made plastic electrochemical-optical cell equipped with front quartz glass [35]. Three electrodes system was used for measurements (working electrode—either ZnO or ZnO-PDA, Pt counter electrode and reference Ag/AgCl, Cl<sup>-</sup><sub>sat.</sub> electrode). The ZnO-PDA samples were excited by UV LED (325 nm, 4 mW, 15 nm full width at half maximum (FWHM)). An optical glass filter was used to cut out noise LED emission in the visible range.

Cyclic voltammetry measurements were performed in the potential range from −500 mV to −800 mV with a scanning speed of 50 mV. Photoluminescence signal was recorded by fiber optic spectrometer Ocean Optics HR4000 (USA). When the sample was installed into an electrochemical cell, the potential was applied, and simultaneous PL measurements were performed. Samples were not moved during the measurements. PL spectra were measured from the same spot after sample installation in the cell. Chronoamperometry tests were performed in combination with PL measurements: a long pulse with constant

potential was applied for 80 s [35]. PL spectra and kinetics at the PL peak position were simultaneously measured.

### 2.5. Electrochemical Impedance Spectroscopy (EIS) Measurements

Electrochemical impedance spectra were recorded in potentiostatic mode by applying a constant potential of  $-0.45$  V and  $-0.3$  V to the working electrode (ZnO and ZnO-PDA). The reference electrode was Ag,AgCl/Cl<sup>-</sup><sub>sat.</sub>, counter electrode—Pt wire. During the registration of electrochemical impedance spectra, the range of alternating current frequencies varied from 0.1 Hz to 100 kHz. The peak-to-peak amplitude of the perturbation voltage was 10 mV. Potentiostat/galvanostat Autolab PGSTAT128N from EcoChemie (Utrecht, The Netherlands) was used for recording EIS data. Registered EIS spectra were evaluated by using EIS data acquisition software “ZView” according to the selected equivalent circuit model applied for the determination of electrochemical characteristics. In this research, EIS data are presented as Nyquist plots where the *x*-axis represents the real impedance component ( $Z'$ ), *y*-axis—is the imaginary impedance component ( $Z''$ ).

### 2.6. Evaluation of Optical and Electrochemical Properties of ZnO-PDA Nanostructures after BSA Incubation

2 mg of BSA was dissolved in 1 mL PBS solution to prepare the stock solution with a concentration of 2 mg/mL. The stock solution was dissolved by PBS to obtain a BSA concentration of 5  $\mu$ g/mL. Twenty microliters of 5  $\mu$ g/mL BSA solution was incubated on the surface of ZnO-PDA nanostructures for 20 min at room temperature. After immobilization, the ZnO-PDA surface was washed three times with PBS.

Photoluminescence and photoelectrochemical properties of ZnO-PDA have been investigated before and after BSA deposition by photoluminescence and cyclic voltammetry methods.

## 3. Results and Discussion

SEM-image of ZnO nanorods shows vertical rods with an average diameter of 50–60 nm and a length of 500 nm (Figure 1A). ZnO nanorods coated with polydopamine are shown in Figure 1B. A change in the color of the nanorods and black formations between them indicates a layer of polydopamine on the surface. Large particles are also observed, which can be explained by polydopamine agglomerations. FTIR is a powerful method to evaluate forming of an interface between organic and inorganic materials. FTIR spectra of ZnO and ZnO-PDA nanostructures are shown in Figure 2.

FTIR spectra of ZnO showed absorption bands in the range of 400, 600 and 800  $\text{cm}^{-1}$ , revealing Zn-O vibrations in ZnO crystal, surface and defect vibrational modes, respectively [37]. After coating ZnO nanorods with polydopamine, FTIR spectroscopy revealed peaks with wave numbers 1187  $\text{cm}^{-1}$ , 1283  $\text{cm}^{-1}$ , 1498  $\text{cm}^{-1}$ , 1595  $\text{cm}^{-1}$ , 3323  $\text{cm}^{-1}$ , which correspond to C-O stretching vibration in the aromatic ring, C-O, C=N or/and C=C, C=O and -OH or/and N-H vibrational modes, respectively. Similar peaks (1288  $\text{cm}^{-1}$ , 1492  $\text{cm}^{-1}$ , 1607  $\text{cm}^{-1}$ , and 3362  $\text{cm}^{-1}$ ) were also previously reported [14,38,39]. The difference between the peak positions (5–30  $\text{cm}^{-1}$ ) compared to the previous results can be connected to the use of different protocols for the synthesis of polydopamine. The studied FTIR absorbance value increased in relation to the concentration of polydopamine in the coating layer, however, the layers were conformal. Deposition conditions (such as the method of deposition, water purification, deposition temperature, storage of dopamine and dopamine producer) can affect the quality of the PDA layer. Additionally, the surface for PDA deposition plays an important role. Fabrication of PDA on glassy carbon electrodes have been performed by electrochemical polymerization, which makes the properties of the PDA different due to the chemical properties of the surface (work function, surface charge and functional groups).

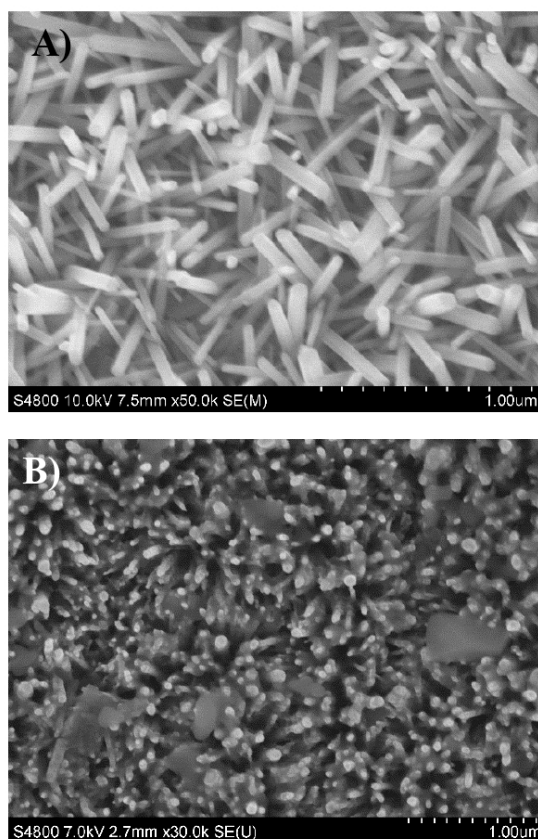


**Figure 1.** SEM of deposited ZnO nanostructures (A) and ZnO-PDA 0.3 mg/mL nanostructures (B).

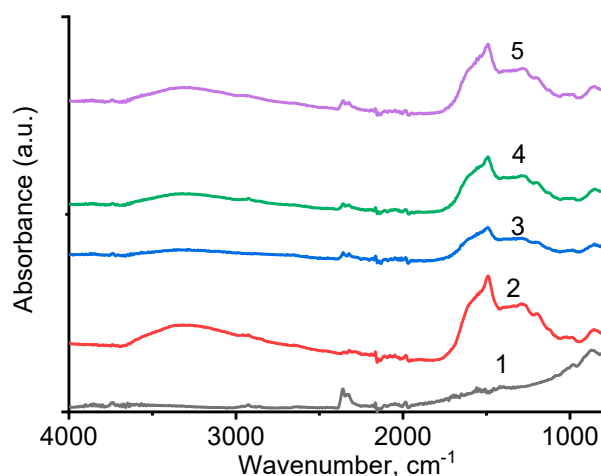


**Figure 2.** FTIR of ZnO and ZnO–PDA nanostructures: 1–ZnO, 2–ZnO-PDA 0.3 mg/mL, 3–ZnO-PDA 0.4 mg/mL, 4–ZnO-PDA 0.5 mg/mL, 5–ZnO-PDA 0.7 mg/mL.

Photoelectrochemical spectroscopy (PES) is a method that enables an investigation of charge transfer phenomena on electrode surfaces. PES can be combined with the photoluminescence method to analyze the dynamics of photoinduced processes more in detail.

Cyclic voltammetry results of ZnO and ZnO-PDA nanostructures, formed at different concentrations of PDA in dark (light off) and UV excitation (light on) are shown in Figure 3. Role of the PDA layer, deposited at different concentrations was analyzed. Despite, PDA is not conductive material, the increase of current compared to bare ZnO was observed for all tested ZnO-PDA samples (Figure 3A). The current value decreased with the increase



of PDA concentration. Excitation of the samples with UV light showed similar results (Figure 3B).

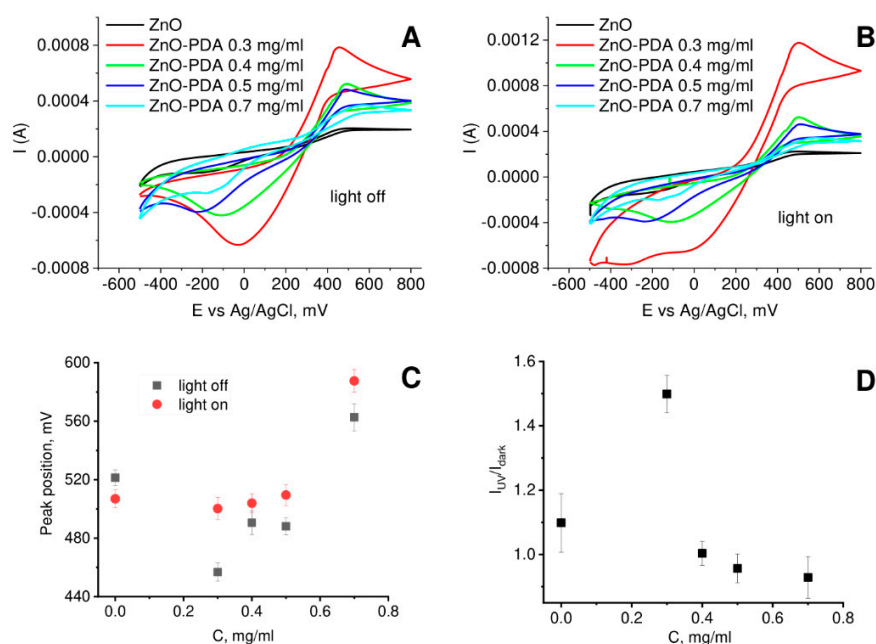


**Figure 3.** Results of electrochemical measurements: Cyclic voltammograms of ZnO electrodes modified with different dopamine concentrations (at 'light off' mode) (A); Cyclic voltammograms of ZnO electrodes modified with different dopamine concentrations (at 'light on' mode) (B); Oxidation peak positions at light off and light on modes (C); Light on/light off peak current ratio (D).

In both CVs (Figure 3A,B), ZnO-PDA nanostructures showed an oxidation peak in the range between 400 mV and 550 mV and a reduction peak in the range between  $-200$  mV and 0 mV. CVs of PDA 0.5 mg/mL are shown in Figure 3C. It was determined a shift of oxidation peak towards higher voltages under UV excitation. PDA layer thickness significantly impacted the ratio of UV current and dark current. This value was higher than 1 for ZnO and ZnO-PDA 0.3 mg/mL. The increase in dopamine concentration resulted in a decrease in the current ratio (Figure 3D).

In the present work, the oxidation peak potential values were 50–80 mV higher than that for PDA layers, reported in the literature [40,41]. It might be due to different methods of PDA synthesis. However, the dynamics of CVs change with the increase in dopamine concentration, which points to the role of the ZnO-PDA interface in this photoelectrochemical process. The obtained results reveal charge trapping and electric field impact to CV in the ZnO-PDA interface. The mechanisms of charge transfer within the interface ZnO-PDA in the dark and in UV conditions are under discussion [2]. In our previous work, it has been proposed that the photogenerated charge in ZnO-PDA is split at the interface in between ZnO and PDA, revealing the quenching of integrated PL intensity the range 360–800 nm [2]. Based on this assumption, an increase of photocurrent was expected. However, on the basis of the results, presented in Figure 2, this assumption was incomplete.

It is reported that PDA DC conductivity is formed by free holes. Humid atmosphere results in 5 order increase of the PDA conductivity [42]. Deposition of PDA over conductive surface reduces the electrical conductivity by a few orders of the magnitude [43]. It was reported that thermal conductivity of Cu-PDA depends on PDA layer thickness. The thermal conductivity decreased with PDA layer thickness. The decrease in thermal conductivity was explained by scattering of electrons in metal by PDA coating [43]. It was reported that in CeO<sub>2</sub>-PDA composites, electrical conductivity increased in a humid

atmosphere [44]. The phenomena was explained by the effect of ionic conductivity in PDA [44].

On the basis of the above-mentioned results, we can propose the increase of oxidation and reduction peak currents of FTO-ZnO-PDA electrodes after the formation of thin PDA layer, which increased ionic conductivity of formed ZnO-PDA structures that were assessed in water-based solutions. The increase of the PDA layer results in reduction of the oxidation and reduction peak currents of FTO-ZnO-PDA electrodes. UV-light generates electron-hole couples on ZnO. On the other hand, UV light can be partially absorbed by the PDA layer [2]. The reduction of oxidation and reduction peak currents of FTO-ZnO-PDA electrodes under UV irradiation can be resulted by electron trapping and recombination with holes in PDA layer. Therefore, PDA layer is necessary for such constructs. Based on previous research [14], the PDA layer thickness can vary between 6–10 nm for dopamine concentrations of 0.3–0.7 mg/mL.

Results on photoluminescence-chronoamperometry study are shown in Figure 4. It was determined that the PL of ZnO-PDA decreased under applied potential (Figure 4A). The electrochromic effect, based on shift of PL peak was firstly determined for ZnO (Figure 4A) [45]. The assessment of the electrochromic effect of ZnO-PDA nanostructures at different dopamine concentrations is shown in Figure 4B,C. It was determined that the PL intensity was reduced by PL-quenching at all dopamine concentrations in the range of all applied potentials. Saturation of the intensity was observed in the range of 600–800 mV. The shift of the PL peak position was observed in the range of 100–500 mV. At higher applied potentials, the saturation of the PL peak shift was observed. The most significant effects of the peak shift and PL intensity decrease were observed for FTO-electrodes ( $19 \times 12 \text{ mm}^2$ ) modified with ZnO-PDA, deposited at dopamine concentration of 0.4 mg/mL and 0.5 mg/mL. It is worth to note that no shift of PL peak was observed for FTO-electrodes modified by ZnO nanostructures not-coated with PDA under any applied potential.

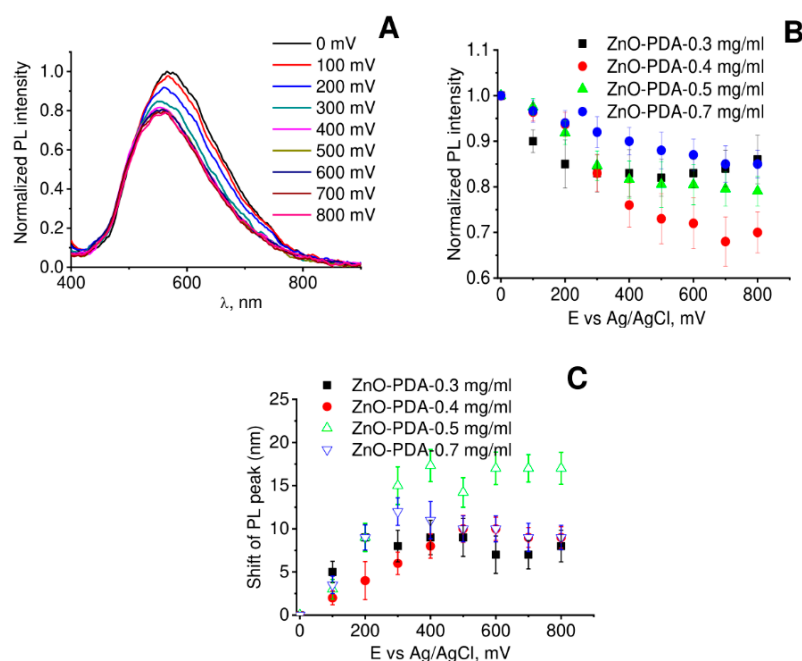


**Figure 4.** Chronoamperometry based evaluation of FTO-electrode modified by ZnO-PDA 0.4 mg/mL nanostructures at different potentials: PL quenching at different applied potentials (A); PL intensity quenching at different applied potentials (B); PL shift at different applied potentials (C).

### 3.1. Characterisation of ZnO and ZnO-PDA with Electrochemical Impedance Spectroscopy

Considering that FTO-electrodes modified with ZnO-PDA layer were investigated by cyclic voltammetry (Figure 3), further experiments were carried out to investigate these electrodes at potentiostatic conditions by using EIS under the applied cathodic potentials of

−0.3 V and −0.45 V vs. Ag/AgCl,Cl<sup>−</sup><sub>sat</sub>. These conditions of cathodic polarization enabled to avoid possible oxidative stress at the working electrode that could cause undesirable deterioration of ZnO and PDA films if anodic potentials would be applied. Additionally, the impedance spectral characterization at the equilibrium potential (0 V vs. Ag/AgCl,Cl<sup>−</sup><sub>sat</sub>) i.e., in the absence of the applied potential, was conducted to better ascertain the effect of the electrical potential on the electrochemical characteristics of ZnO and ZnO-PDA electrodes. The Nyquist plot in Figure 5A illustrates that the electrochemical impedance of the FTO-ZnO electrode strongly depends on the applied potential independently on lighting. Calculated values of the parameters (Table 1) of modelling equivalent circuit (Figure 5A, inset) showed that (i) charge transfer resistance ( $R_{ct}$ ) decreases from approx. 35 kΩ cm<sup>2</sup> to 5.6 kΩ cm<sup>2</sup> when the electrode is polarized more negatively (Figure 5B, black columns) and (ii)  $R_{ct}$  slightly decreases when the FTO-ZnO electrode is lit under −0.3 V potential, however at −0.45 V  $R_{ct}$  does not depend on lighting (Figure 5B, white columns). The values of constant phase element (CPE) almost do not depend on lighting as well, however, CPE increases from approx. 164 μF/cm<sup>2</sup> to 221 μF/cm<sup>2</sup> when the FTO-ZnO electrode is polarized more negatively (Figure 5C). Summarizing the data presented in Figure 4 we conclude that the impedance of the FTO-ZnO electrode strongly depends on the applied cathodic potential, and slightly depends on lighting. These results clearly demonstrate that by using −0.45 V electrode potential faster charge transfer can be achieved through the interface electrode-electrolyte than by using −0.3 V. Meanwhile under equilibrium conditions (at 0 V vs. Ag/AgCl,Cl<sup>−</sup><sub>sat</sub>) i.e., in the absence of the applied potential, the shape of Nyquist plot (Figure 5D) do not show clearly expressed semicircle that can be related to some charge transfer limitations. Therefore, the equivalent circuit model with the additional element of CPE2 (Figure 5D, inset) was used to evaluate the individual components of the EIS for FTO-ZnO electrode at equilibrium conditions. Although in this case a decrease in resistance and capacitance was observed (Figure 5E,F) when the electrode is lit, these results cannot be directly compared with the results obtained under −0.45 V and −0.3 V potentials, as the data modelling required the use of an equivalent scheme in which  $R_{ct}$  is connected in series with the CPE2, i.e., it would be inappropriate to correlate the calculated parameters. However, it can be concluded from the obtained EIS data that the total impedance of the FTO-ZnO electrode under equilibrium conditions is significantly higher than under conditions of −0.45 V and −0.3 V, indicating that at 0 V strong limitations of charge transfer occur across the interface between the electrode and PBS.

**Table 1.** Values of modelled parameters of impedance spectra of the FTO-ZnO electrode (Figure 5A,D) at different potentials vs. Ag/AgCl,Cl<sup>−</sup><sub>sat</sub>, according to equivalent circuit model presented in Figure 5A,D insets. An error (%) for each calculated parameter is presented in brackets.

E, V		−0.45	−0.3	0
Light off	$R_0$ , Ω cm <sup>2</sup>	161.3 (0.3%)	164 (0.4%)	172 (0.5%)
	$R_{ct}$ , kΩ cm <sup>2</sup>	5.6 (1.8%)	35.6 (6.8%)	4.1 (43%)
	$CPE_1$ , μF/cm <sup>2</sup>	221.6 (0.9%)	164.4 (0.8%)	32.6 (7.5%)
	$n$	0.73 (0.4%)	0.74 (0.4%)	0.8 (1.3%)
	$CPE_2$ , μF/cm <sup>2</sup>	-	-	21.8 (10.3%)
	$n$	-	-	0.6 (2.1%)
Light on	$R_0$ , Ω cm <sup>2</sup>	161.8 (0.4%)	162.4 (0.5%)	170 (0.6%)
	$R_{ct}$ , kΩ cm <sup>2</sup>	5.56 (2.0%)	29.7 (8.0%)	2.4 (38%)
	$CPE_1$ , μF/cm <sup>2</sup>	218.0 (1.1%)	168.5 (1.2%)	28.7 (9%)
	$n$	0.73 (0.4%)	0.72 (0.5%)	0.8 (1.6%)
	$CPE_2$ , μF/cm <sup>2</sup>	-	-	36.3 (6.5%)
	$n$	-	-	0.6 (1.8%)



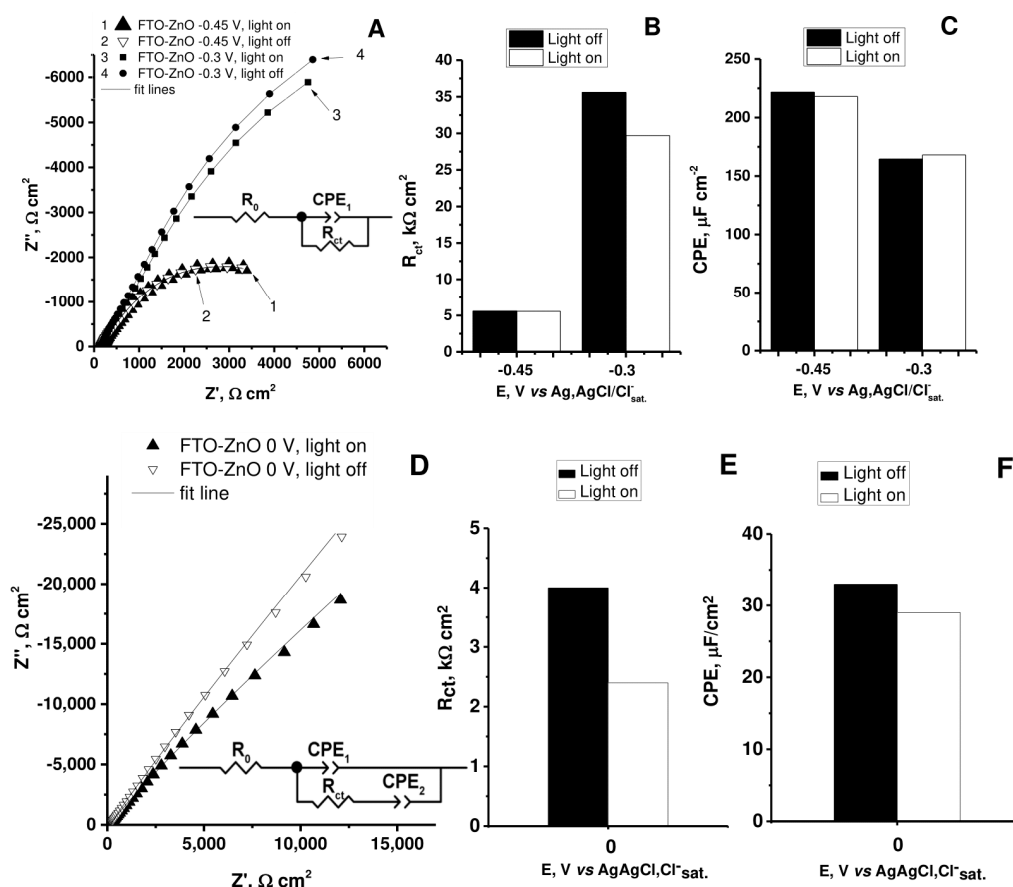


**Figure 5.** Electrochemical impedance spectra of the FTO-ZnO electrode registered at  $-0.3$  and  $-0.45$  V (A),  $0$  V (D) potentials vs.  $Ag/AgCl, Cl^-_{sat}$  with light off or on; inset of A represents equivalent circuit, that impedance data were fitted to:  $R_0$ —resistance of the solution,  $CPE$ —constant phase element,  $R_{ct}$ —charge transfer resistance; inset of D represents equivalent circuit, that impedance data were fitted to:  $R_0$ —resistance of the solution,  $CPE_1$  and  $CPE_2$ —constant phase elements,  $R_{ct}$ —charge transfer resistance. Comparison of modelled parameters— $R_{ct}$  (B,E) and CPE (C,F) according to equivalent circuits presented in insets of A,D.

Electrochemical impedance spectra were registered by using the FTO-ZnO-PDA electrode (Figure 6) to elucidate the influence of deposited PDA layer formed at  $0.4$  mg/mL of dopamine. In contrary to the FTO-ZnO electrode, the impedance of PDA covered electrode only slightly depends on the applied potential, and very slightly depends on lighting. By fitting experimental data (Figure 6A) using equivalent circuit (Figure 6A, inset) kinetic parameters were calculated and are presented in Table 2. Figure 6B,C illustrates the same tendency of calculated electrochemical parameters as it was obtained for the FTO-ZnO electrode (Figure 5).  $R_{ct}$  decreases when the FTO-ZnO-PDA electrode is lit and polarized more negatively (Figure 6B), and  $CPE_1$  decreases when the electrode is lit and increases when the electrode is polarized more negatively (Figure 6C).

However, it should be noted that total system resistance of the FTO-ZnO-PDA electrode decreased approx. twice at  $-0.45$  V and tenfold at  $-0.3$  V electrode potential, in comparison to the FTO-ZnO electrode indicating that PDA layer acts as conductive material, and this finding agrees with the results of CV-based experiments presented in Figure 3A,B.

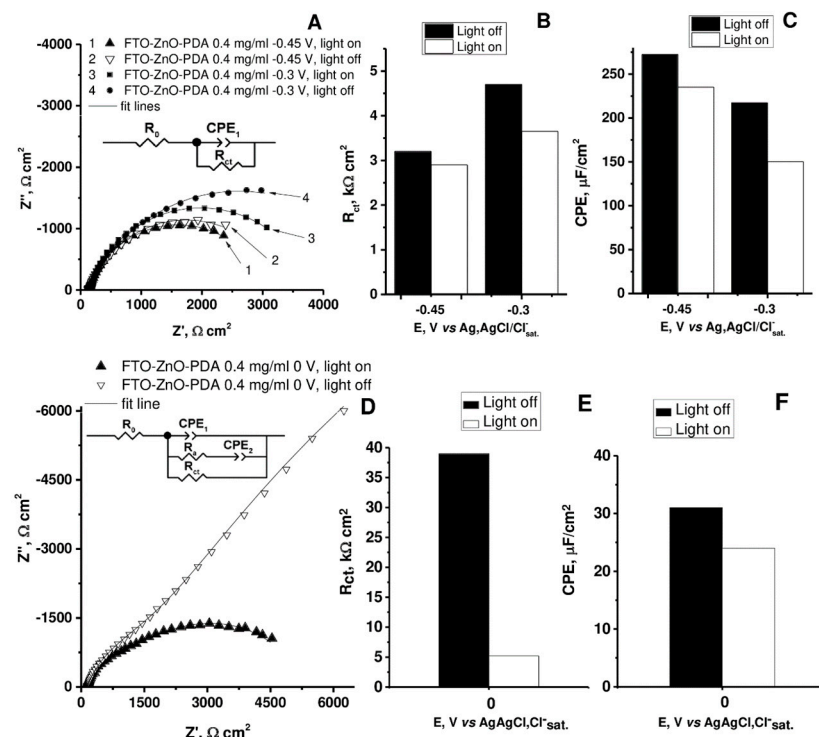


**Figure 6.** Electrochemical impedance spectra of the FTO-ZnO-PDA electrode registered at  $-0.3$  and  $-0.45$  V (A),  $0$  V (D) potentials (*vs* Ag/AgCl, Cl<sup>−</sup><sub>sat.</sub>) in ‘light off’ or ‘light on’ mode; inset of (A) represents equivalent circuit, which was used for the assessment of impedance spectroscopy data:  $R_0$ —resistance of the solution,  $CPE$ —constant phase element,  $R_{ct}$ —charge transfer resistance; inset of (D) represents equivalent circuit, which was used for the assessment of impedance spectroscopy data:  $R_0$ —resistance of the solution,  $CPE_1$  and  $CPE_2$ —constant phase elements,  $R_a$ —adsorption resistance,  $R_{ct}$ —charge transfer resistance. Comparison of modelled parameters— $R_{ct}$  (B,E) and  $CPE$  (C,F) calculated according to equivalent circuits presented in insets of (A,D).

**Table 2.** Values of modelled parameters of impedance spectra of the FTO-ZnO-PDA electrode (Figure 6A) according to equivalent circuit in Figure 6A,D insets. An error (%) for each calculated parameter is presented in brackets.

$E, V$		$-0.45$	$-0.3$	$0$
Light off	$R_0, \Omega \text{ cm}^2$	135.6 (0.5%)	138.7 (0.6%)	138 (0.6%)
	$R_{ct}, \text{k}\Omega \text{ cm}^2$	3.2 (1.9%)	4.7 (2.3%)	39.5 (13.8%)
	$CPE_1, \mu\text{F}/\text{cm}^2$	272.2 (1.3%)	217.2 (1.4%)	30.7 (4.5%)
	$n$	0.78 (0.6%)	0.76 (0.6%)	0.8 (0.9%)
	$R_a$	-	-	3.1 (8.6%)
	$CPE_2$	-	-	81 (5.6%)
	$n$	-	-	0.7 (3.9%)
	Light on	$R_0, \Omega \text{ cm}^2$	134.4 (0.7%)	138 (0.7%)
$R_{ct}, \text{k}\Omega \text{ cm}^2$		2.9 (2.3%)	3.6 (1.2%)	5.2 (3.1%)
$CPE_1, \mu\text{F}/\text{cm}^2$		235.1 (1.9%)	150.1 (2.1%)	24.1 (7.1%)
$n$		0.79 (0.7%)	0.81 (0.7%)	0.8 (1.2%)
$R_a$		-	-	2.8 (14.8%)
$CPE_2$		-	-	57.6 (11.4%)
$n$		-	-	0.7 (6.3%)

Under equilibrium conditions, the shapes of Nyquist plot of the FTO-ZnO-PDA electrode strongly depend on the applied lighting (Figure 6D), however the satisfactory fit results were obtained by using the equivalent circuit model with additional elements of absorption resistance ( $R_a$ ) and adsorption capacitance ( $CPE2$ ). It can be seen (Figure 6E,F) that values of  $R_{ct}$  drastically decreases from  $39.5 \text{ k}\Omega \text{ cm}^2$  to  $5.5 \text{ k}\Omega \text{ cm}^2$  when the electrode is lit. These data show that the influence of lighting on the electrochemical behaviour of the FTO-ZnO-PDA electrode under equilibrium conditions (at  $0 \text{ V vs. Ag/AgCl, Cl}^-_{\text{sat}}$ ) is very high. However, the absolute values of  $R_{ct}$  when the electrode is lit, varies in a relatively narrow range from  $2.9 \text{ k}\Omega \text{ cm}^2$  to  $5.2 \text{ k}\Omega \text{ cm}^2$  independently on the applied potential.

In conclusion, EIS data showed that the values of charge transfer resistance are higher for the FTO-ZnO electrode than for the FTO-ZnO-PDA electrode regardless of lighting or the applied cathodic potential of  $-0.3 \text{ V}$  or  $-0.45 \text{ V vs. Ag/AgCl, Cl}^-_{\text{sat}}$ . This finding indicates that the charge transfer rate at the interface between FTO-ZnO electrode and buffer solution can be increased by modifying the electrode with the PDA layer formed at  $0.4 \text{ mg/mL}$  of dopamine. It is important to note that charge transfer resistance ( $R_{ct}$ ) at the FTO-ZnO-PDA electrode—buffer solution interface depends on the applied potential, because experimental results of this study (Figures 5 and 6, Tables 1 and 2) showed that  $R_{ct}$  decreased approximately twice by applying  $-0.45 \text{ V}$  electrode potential, however it decreased even tenfold by applying  $-0.3 \text{ V vs. Ag/AgCl, Cl}^-_{\text{sat}}$  electrode potential.

EIS measurements under equilibrium conditions (at  $0 \text{ V vs. Ag/AgCl, Cl}^-_{\text{sat}}$ ) showed that the total impedance of the FTO-ZnO electrode is significantly higher than under conditions of  $-0.45 \text{ V}$  and  $-0.3 \text{ V}$ , indicating strong limitations of charge transfer across the interface between the electrode and PBS in the absence of the applied potential. Meanwhile, EIS measurements under equilibrium conditions by using the FTO-ZnO-PDA electrode showed a very high influence of lighting on the electrochemical behaviour of the electrode. However, the absolute values of  $R_{ct}$  can be considered as similar independently on the applied potential when the electrode is lit.

### 3.2. Characterisation of ZnO-PDA Interaction with BSA Molecules by Photoluminescence and Photoelectrochemical Methods

Cyclic voltammograms results of ZnO-PDA nanostructures in dark and light excitation before and after BSA incubation are shown in Figure 7. It was found that adsorption of BSA molecules on the ZnO-PDA surface resulted in a significant decrease of the current value. The oxidation peak shifted to higher values after BSA adsorption. Light excitation didn't increase the electrochemical signal significantly.

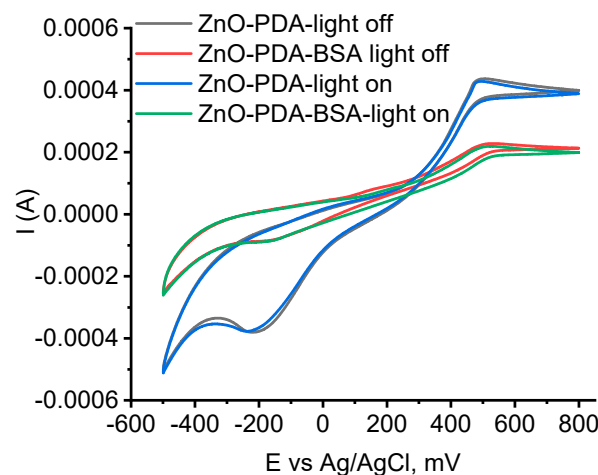


**Figure 7.** Cyclic voltammograms of FTO–ZnO–PDA–0.5 mg/mL nanostructures in dark and light excitation conditions, measured before and after immobilization of BSA.

Photoluminescence spectra of FTO-ZnO-PDA nanostructures, measured before and after BSA incubation are shown in Figure 8. Photoluminescence spectra without applied

potential before and after BSA adsorption are shown in Figure 8A. It was found, that BSA adsorption resulted in quenching of the photoluminescence intensity and red shift of visible peak of FTO-ZnO-PDA emission (Figure 8A).

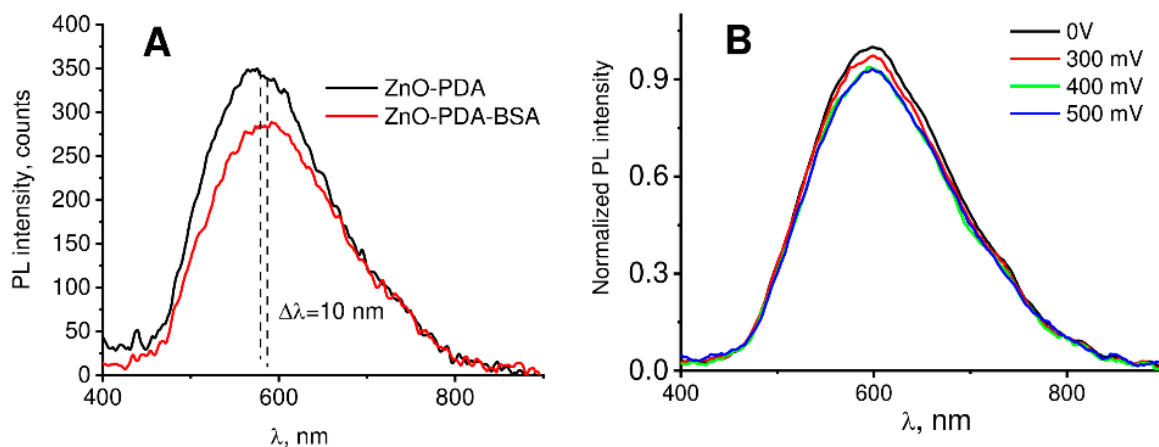


**Figure 8.** Photoluminescence spectra of FTO–ZnO–PDA–0.5 mg/mL nanostructures: (A) before and after immobilization of BSA without applied potential; (B) after immobilization of BSA with applied potential.

Photoluminescence spectra with applied potential after BSA adsorption are shown in Figure 7B. It was found, that after BSA adsorption, low applied potentials (100–200 mV) didn't change intensity and peak position of PL spectra. An increase of the applied potential resulted in a decrease of PL intensity. At applied potentials, higher than 500 mV, no changes of the PL signal were observed (Figure 8B).

We can propose the model of photoelectrochemical processes at ZnO-PDA interface, shown in Figure 9. When the electrochemical potential  $E_1$  is applied to the ZnO-PDA electrode, the photogenerated charges are split within this field. We proved the presence of the local field  $E_2$  at the interface between ZnO and PDA components [14]. Additional charge diffusion towards interface solution-PDA-ZnO is expected at the applied electrochemical potential. As a result, the local field  $E_3$  will be formed. It will stimulate charge separation and PL quenching.

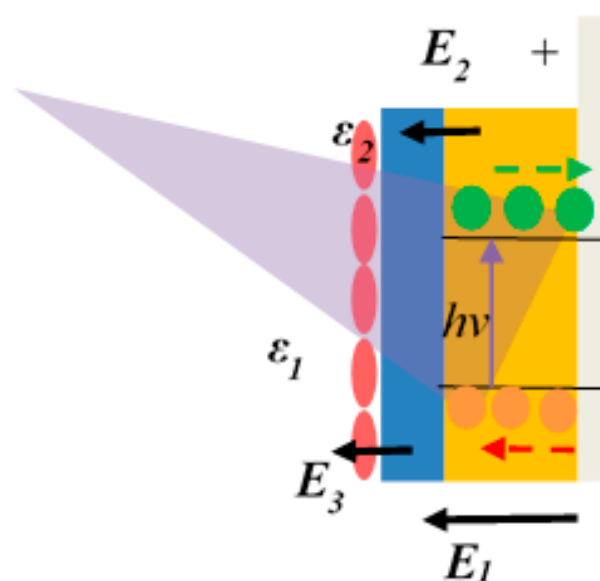


**Figure 9.** Scheme of possible photoelectrochemical processes on FTO-ZnO-PDA-BSA interface.  $E_1$ —electrochemical potential,  $E_2$ —local field,  $E_3$ —new local field,  $\epsilon_1$ ,  $\epsilon_2$ —dielectric permittivity of different layers.

ZnO nanostructures have different types of photoluminescence defects (Zn/O vacancies and interstitials) [14]. Under applied electrochemical potential, the local field might result in an increase of depletion layer at the ZnO surface and charge transfer from ZnO centers of luminescence to the surface states [46]. In the present paper, PDA layer plays an important role, as it forms additional surface states on the ZnO surface. The applied potential stimulates charge transitions between the ZnO defect state and PDA-formed states. This results in a peak shift of photoluminescence under applied potential.

Adsorption of biomolecules on the ZnO-PDA surface makes the processes of charge transfer more complicated. The adsorbed BSA molecules form an additional surface layer with dielectric permittivity  $\epsilon_2$  ( $\epsilon_2 \neq \epsilon_1$ ) (Figure 8). We assume two possible effects on the FTO-ZnO-PDA-interface: charge transfer between the adsorbed BSA molecules and ZnO-PDA surface and change of local field  $E_3$ . Previously, it was proposed the interaction model for metal oxide-biomolecule interaction [47]. The local field, formed by biomolecules on the surface of the metal oxide, was responsible for the change in optical and electrical properties [47]. Interaction between BSA and ZnO surface was assisted with the change of photoluminescence intensity due to the local field formed by BSA molecules [48,49]. Thus, BSA molecules could form a shielding layer, restricting the diffusion of the ions from the electrolyte.

The latter stimulates a lower response of the sample's PL signal to the applied electrochemical potential.

#### 4. Conclusions

In this paper, ZnO nanorods were formed on the surface of FTO that was further modified with PDA layers. The formation of ZnO nanorods was confirmed by SEM and FTIR measurements. Formation of PDA layers by polymerization of dopamine increased sensitivity towards UV light. It was observed that currents of oxidation and reduction processes are dependent on lighting, and relevant shifts of peak currents were determined in CV measurements under UV light. Electrochemical properties also depended on the concentration of PDA. It was determined that it is possible to manipulate the intensity of photoluminescence peaks by changing bias potential. Electrochemical impedance spectroscopy measurements showed that modification of the FTO-ZnO electrode with the PDA layer results in a significant decrease of charge transfer resistance at the electrode-buffer solution interface, indicating that the FTO-ZnO-PDA electrode acts as more conductive material than the FTO-ZnO electrode. EIS data analysis showed that electrochemical parameters of both FTO-ZnO and FTO-ZnO-PDA electrodes could be manipulated by changing the electrode polarization and the lighting as well. Hence, in this work, we have demonstrated that the properties of ZnO can be changed/tuned by depositing a polydopamine (PDA) layer, which enables the advanced application of ZnO-PDA structures for immobilization of biomaterials, such as BSA. The observed change of PL peak intensity after immobilization of BSA demonstrates the applicability of the FTO-ZnO-PDA electrode in the design of sensors and/or other technological tools.

**Author Contributions:** Conceptualization, R.V., A.V. and A.R.; Methodology, A.V., V.F. and I.G.; Software, I.G.; Validation, V.H., V.F., A.V. and I.T.; Formal Analysis, A.V., V.F. and S.R.; Investigation, I.G. and I.T.; Resources, R.V., V.H. and A.R.; Data Curation, A.V., R.V. and A.R.; Writing—Original Draft Preparation, R.V., V.F., S.R. and I.G.; Writing—Review & Editing, A.V., S.R. and A.R.; Visualization, I.G., V.H. and V.F.; Supervision, A.V., R.V. and A.R.; Project Administration, R.V. and A.R.; Funding Acquisition, R.V. and A.R. All authors have read and agreed to the published version of the manuscript.

**Funding:** This work was supported by: EU Horizon 2020 research and innovation programme H2020-MSCA-RISE under grant agreement № 778157 CanBioSe, Ukraine-Latvia bilateral project “Development of nanostructured optical sensor system for detection of K. Pneumonia” (LV-UA/2021/2). Funded by **Latvian Council of Science**; “ZnO/porfirīna nanokompozītu izstrāde optiskiem nanosensoriem gaistošo organisko savienojumu noteikšanai”. Project Nr. 1.1.1.2/VIAA/3/19/490. Funded by **Latvian Council of Science**.



**Institutional Review Board Statement:** Not applicable.

**Informed Consent Statement:** Not applicable.

**Data Availability Statement:** Data available by request.

**Conflicts of Interest:** The authors declare no conflict of interest.

## References

1. German, N.; Popov, A.; Ramanavicius, A.; Ramanaviciene, A. Development and Practical Application of Glucose Biosensor Based on Dendritic Gold Nanostructures Modified by Conducting Polymers. *Biosensors* **2022**, *12*, 641. [[CrossRef](#)]
2. Fedorenko, V.; Viter, R.; Mrówczyński, R.; Damberg, D.; Coy, E.; Iatsunskyi, I. Synthesis and photoluminescence properties of hybrid 1D core-shell structured nanocomposites based on ZnO/polydopamine. *RSC Adv.* **2020**, *10*, 29751–29758. [[CrossRef](#)] [[PubMed](#)]
3. Dutt, A.; Matsumoto, Y.; Santana-Rodríguez, G.; Ramos, E.; Monroy, B.M.; Salazar, J.S. Surface chemistry and density distribution influence on visible luminescence of silicon quantum dots: An experimental and theoretical approach. *Phys. Chem. Chem. Phys.* **2017**, *19*, 1526–1535. [[CrossRef](#)] [[PubMed](#)]
4. Matsumoto, Y.; Dutt, A.; Santana-Rodríguez, G.; Santoyo-Salazar, J.; Aceves-Mijares, M. Nanocrystalline Si/SiO<sub>2</sub> core-shell network with intense white light emission fabricated by hot-wire chemical vapor deposition. *Appl. Phys. Lett.* **2015**, *106*, 171912. [[CrossRef](#)]
5. González-Garnica, M.; Galdámez-Martínez, A.; Malagón, F.; Ramos, C.; Santana, G.; Abolhassani, R.; Panda, P.K.; Kaushik, A.; Mishra, Y.K.; Karthik, T.V.; et al. One dimensional Au-ZnO hybrid nanostructures based CO<sub>2</sub> detection: Growth mechanism and role of the seed layer on sensing performance. *Sens. Actuators B Chem.* **2021**, *337*, 129765. [[CrossRef](#)]
6. Matlou, G.G.; Abrahamse, H. Hybrid Inorganic-Organic Core-Shell Nanodrug Systems in Targeted Photodynamic Therapy of Cancer. *Pharmaceutics* **2021**, *13*, 1773. [[CrossRef](#)] [[PubMed](#)]
7. Kalambate, P.K.; Dhanjai; Huang, Z.; Li, Y.; Shen, Y.; Xie, M.; Huang, Y.; Srivastava, A.K. Core@shell nanomaterials based sensing devices: A review. *TrAC Trends Anal. Chem.* **2019**, *115*, 147–161. [[CrossRef](#)]
8. Lv, X.-W.; Hu, Z.-P.; Chen, L.; Ren, J.-T.; Liu, Y.-P.; Yuan, Z.-Y. Organic-Inorganic Metal Phosphonate-Derived Nitrogen-Doped Core-Shell Ni<sub>2</sub>P Nanoparticles Supported on Ni Foam for Efficient Hydrogen Evolution Reaction at All pH Values. *ACS Sustain. Chem. Eng.* **2019**, *7*, 12770–12778. [[CrossRef](#)]
9. Khodadadi, B.; Bordbar, M.; Nasrollahzadeh, M. Green synthesis of Pd nanoparticles at Apricot kernel shell substrate using Salvia hydrangea extract: Catalytic activity for reduction of organic dyes. *J. Colloid Interface Sci.* **2017**, *490*, 1–10. [[CrossRef](#)]
10. Ge, F.; Ye, H.; Li, M.-M.; Zhao, B.-X. Efficient removal of cationic dyes from aqueous solution by polymer-modified magnetic nanoparticles. *Chem. Eng. J.* **2012**, *198–199*, 11–17. [[CrossRef](#)]
11. Moustakas, N.; Kontos, A.; Likodimos, V.; Katsaros, F.; Boukos, N.; Tsoutsou, D.; Dimoulas, A.; Romanos, G.; Dionysiou, D.; Falaras, P. Inorganic-organic core-shell titania nanoparticles for efficient visible light activated photocatalysis. *Appl. Catal. B Environ.* **2012**, *130–131*, 14–24. [[CrossRef](#)]
12. Li, J.-Y.; Jiang, X.; Lin, L.; Zhou, J.-J.; Xu, G.-S.; Yuan, Y.-P. Improving the photocatalytic performance of polyimide by constructing an inorganic-organic hybrid ZnO-polyimide core-shell structure. *J. Mol. Catal. A Chem.* **2015**, *406*, 46–50. [[CrossRef](#)]
13. Tavakoli, S.; Kharaziha, M.; Nemati, S. Polydopamine coated ZnO rod-shaped nanoparticles with noticeable biocompatibility, hemostatic and antibacterial activity. *Nano-Struct. Nano-Objects* **2021**, *25*, 100639. [[CrossRef](#)]
14. Fedorenko, V.; Damberg, D.; Grundsteins, K.; Ramanavicius, A.; Ramanavicius, S.; Coy, E.; Iatsunskyi, I.; Viter, R. Application of Polydopamine Functionalized Zinc Oxide for Glucose Biosensor Design. *Polymers* **2021**, *13*, 2918. [[CrossRef](#)] [[PubMed](#)]
15. Damberg, D.; Fedorenko, V.; Grundsteins, K.; Altundal, Ş.; Šutka, A.; Ramanavičius, A.; Coy, E.; Mrówczyński, R.; Iatsunskyi, I.; Viter, R. Influence of PDA Coating on the Structural, Optical and Surface Properties of ZnO Nanostructures. *Nanomaterials* **2020**, *10*, 2438. [[CrossRef](#)] [[PubMed](#)]
16. Ramanaviciene, A.; German, N.; Kausaite-Minkstimiene, A.; Voronovic, J.; Kirlyte, J.; Ramanavicius, A. Comparative study of surface plasmon resonance, electrochemical and electroassisted chemiluminescence methods based immunosensor for the determination of antibodies against human growth hormone. *Biosens. Bioelectron.* **2012**, *36*, 48–55. [[CrossRef](#)] [[PubMed](#)]
17. Valiūnienė, A.; Rekeraitė, A.I.; Ramanavičienė, A.; Mikoliūnaitė, L.; Ramanavičius, A. Fast Fourier transformation electrochemical impedance spectroscopy for the investigation of inactivation of glucose biosensor based on graphite electrode modified by Prussian blue, polypyrrole and glucose oxidase. *Colloids Surf. A Physicochem. Eng. Asp.* **2017**, *532*, 165–171. [[CrossRef](#)]
18. Häcker, J.; Danner, C.; Sievert, B.; Biswas, I.; Zhao-Karger, Z.; Wagner, N.; Friedrich, K.A. Investigation of Magnesium-Sulfur Batteries using Electrochemical Impedance Spectroscopy. *Electrochim. Acta* **2020**, *338*, 135787. [[CrossRef](#)]
19. Baumann, M.; Wildfeuer, L.; Rohr, S.; Lienkamp, M. Parameter variations within Li-Ion battery packs—Theoretical investigations and experimental quantification. *J. Energy Storage* **2018**, *18*, 295–307. [[CrossRef](#)]
20. Oldenburger, M.; Bedürftig, B.; Gruhle, A.; Grimsmann, F.; Richter, E.; Findeisen, R.; Hintennach, A. Investigation of the low frequency Warburg impedance of Li-ion cells by frequency domain measurements. *J. Energy Storage* **2019**, *21*, 272–280. [[CrossRef](#)]
21. Valiūnienė, A.; Kavaliauskaitė, G.; Virbickas, P.; Ramanavičius, A. Prussian blue based impedimetric urea biosensor. *J. Electroanal. Chem.* **2021**, *895*, 115473. [[CrossRef](#)]

22. Gabriunaite, I.; Valincius, G.; Žilinskas, A.; Valiūnienė, A. Tethered Bilayer Membrane Formation on Silanized Fluorine Doped Tin Oxide Surface. *J. Electrochem. Soc.* **2022**, *169*, 037515. [CrossRef]
23. Gabriunaite, I.; Valiūnienė, A.; Sabirovas, T.; Valincius, G. Mixed Silane-based Self-assembled Monolayers Deposited on Fluorine Doped Tin Oxide as Model System for Development of Biosensors for Toxin Detection. *Electroanalysis* **2021**, *33*, 1315–1324. [CrossRef]
24. Sabirovas, T.; VALIŪNIENĖ, A.; Valincius, G. Mechanically Polished Titanium Surface for Immobilization of Hybrid Bilayer Membrane. *J. Electrochem. Soc.* **2018**, *165*, G109–G115. [CrossRef]
25. Riquelme, A.; Bennett, L.J.; Courtier, N.E.; Wolf, M.J.; Contreras-Bernal, L.; Walker, A.B.; Richardson, G.; Anta, J.A. Identification of recombination losses and charge collection efficiency in a perovskite solar cell by comparing impedance response to a drift-diffusion model. *Nanoscale* **2020**, *12*, 17385–17398. [CrossRef] [PubMed]
26. Arredondo, B.; Romero, B.; Beliatas, M.; del Pozo, G.; Martín-Martín, D.; Blakesley, J.; Dibb, G.; Krebs, F.; Gevorgyan, S.; Castro, F. Analysing impact of oxygen and water exposure on roll-coated organic solar cell performance using impedance spectroscopy. *Sol. Energy Mater. Sol. Cells* **2018**, *176*, 397–404. [CrossRef]
27. Omar, A.; Ali, M.S.; Rahim, N.A. Electron transport properties analysis of titanium dioxide dye-sensitized solar cells (TiO<sub>2</sub>-DSSCs) based natural dyes using electrochemical impedance spectroscopy concept: A review. *Sol. Energy* **2020**, *207*, 1088–1121. [CrossRef]
28. Ayagou, M.D.D.; Tran, T.T.M.; Tribollet, B.; Kittel, J.; Sutter, E.; Ferrando, N.; Mendibide, C.; Duret-Thual, C. Electrochemical impedance spectroscopy of iron corrosion in H<sub>2</sub>S solutions. *Electrochim. Acta* **2018**, *282*, 775–783. [CrossRef]
29. Gomes, M.P.; Costa, I.; Pébère, N.; Rossi, J.; Tribollet, B.; Vivier, V. On the corrosion mechanism of Mg investigated by electrochemical impedance spectroscopy. *Electrochim. Acta* **2019**, *306*, 61–70. [CrossRef]
30. De Motte, R.; Basilico, E.; Mingant, R.; Kittel, J.; Ropital, F.; Combrade, P.; Necib, S.; Deydier, V.; Crusset, D.; Marcelin, S. A study by electrochemical impedance spectroscopy and surface analysis of corrosion product layers formed during CO<sub>2</sub> corrosion of low alloy steel. *Corros. Sci.* **2020**, *172*, 108666. [CrossRef]
31. Samukaite-Bubniene, U.; Valiūnienė, A.; Bucinskas, V.; Genys, P.; Ratautaite, V.; Ramanaviciene, A.; Aksun, E.; Tereshchenko, A.; Zeybek, B.; Ramanavicius, A. Towards supercapacitors: Cyclic voltammetry and fast Fourier transform electrochemical impedance spectroscopy based evaluation of polypyrrole electrochemically deposited on the pencil graphite electrode. *Colloids Surf. A Physicochem. Eng. Asp.* **2021**, *610*, 125750. [CrossRef]
32. Larsen, A.; Dahal, E.; Paluba, J.; Cianciulli, K.; Isenhardt, B.; Arnold, M.; Du, B.; Jiang, Y.; White, M.S. Nonlinear impedance spectroscopy of organic MIS capacitors and planar heterojunction diodes. *Org. Electron.* **2018**, *62*, 660–666. [CrossRef]
33. Vicentini, R.; Soares, D.M.; Nunes, W.; Freitas, B.; Costa, L.; Da Silva, L.M.; Zanin, H. Core-niobium pentoxide carbon-shell nanoparticles decorating multiwalled carbon nanotubes as electrode for electrochemical capacitors. *J. Power Sources* **2019**, *434*, 226737. [CrossRef]
34. Bard, A.J.; Faulkner, L.R. *Electrochemical Methods: Fundamentals and Applications*, 2nd ed.; John Wiley and Sons: New York, NY, USA, 2008. Available online: <https://www.wiley.com/en-us/Electrochemical+Methods%3A+Fundamentals+and+Applications%2C+2nd+Edition-p-9780470452530> (accessed on 29 April 2022).
35. Viter, R.; Kunene, K.; Genys, P.; Jevdokimovs, D.; Erts, D.; Sutka, A.; Bisetty, K.; Viksna, A.; Ramanaviciene, A.; Ramanavicius, A. Photoelectrochemical Bisphenol S Sensor Based on ZnO-Nanorods Modified by Molecularly Imprinted Polypyrrole. *Macromol. Chem. Phys.* **2020**, *221*, 1900232. [CrossRef]
36. Tamashevski, A.; Harmaza, Y.; Slobozhanina, E.; Viter, R.; Iatsunskiy, I. Photoluminescent Detection of Human T-Lymphoblastic Cells by ZnO Nanorods. *Molecules* **2020**, *25*, 3168. [CrossRef] [PubMed]
37. Viter, R.; Savchuk, M.; Iatsunskiy, I.; Pietralik, Z.; Starodub, N.; Shpyrka, N.; Ramanaviciene, A.; Ramanavicius, A. Analytical, thermodynamical and kinetic characteristics of photoluminescence immunosensor for the determination of Ochratoxin A. *Biosens. Bioelectron.* **2018**, *99*, 237–243. [CrossRef]
38. Luo, H.; Gu, C.; Zheng, W.; Dai, F.; Wang, X.; Zheng, Z. Facile synthesis of novel size-controlled antibacterial hybrid spheres using silver nanoparticles loaded with poly-dopamine spheres. *RSC Adv.* **2015**, *5*, 13470–13477. [CrossRef]
39. Zhang, S.; Jiang, Z.; Zhang, W.; Wang, X.; Shi, J. Polymer–inorganic microcapsules fabricated by combining biomimetic adhesion and bioinspired mineralization and their use for catalase immobilization. *Biochem. Eng. J.* **2015**, *93*, 281–288. [CrossRef]
40. Amiri, M.; Amali, E.; Nematollahzadeh, A. Poly-dopamine thin film for voltammetric sensing of atenolol. *Sens. Actuators B Chem.* **2015**, *216*, 551–557. [CrossRef]
41. Amiri, M.; Amali, E.; Nematollahzadeh, A.; Salehniya, H. Poly-dopamine films: Voltammetric sensor for pH monitoring. *Sens. Actuators B Chem.* **2016**, *228*, 53–58. [CrossRef]
42. Coskun, H.; Aljabour, A.; Uiberlacker, L.; Strobel, M.; Hild, S.; Cobet, C.; Farka, D.; Stadler, P.; Sariciftci, N.S. Chemical vapor deposition—Based synthesis of conductive polydopamine thin-films. *Thin Solid Film.* **2018**, *645*, 320–325. [CrossRef]
43. Yuan, H.; Wang, Y.; Li, T.; Ma, P.; Zhang, S.; Du, M.; Chen, M.; Dong, W.; Ming, W. Highly thermal conductive and electrically insulating polymer composites based on polydopamine-coated copper nanowire. *Compos. Sci. Technol.* **2018**, *164*, 153–159. [CrossRef]
44. D’Amato, R.; Donnadio, A.; Battocchio, C.; Sassi, P.; Pica, M.; Carbone, A.; Gatto, I.; Casciola, M. Polydopamine Coated CeO<sub>2</sub> as Radical Scavenger Filler for Aquivion Membranes with High Proton Conductivity. *Materials* **2021**, *14*, 5280. [CrossRef] [PubMed]

45. Kim, J.H.; Joshi, M.K.; Lee, J.; Park, C.H.; Kim, C.S. Polydopamine-assisted immobilization of hierarchical zinc oxide nanostructures on electrospun nanofibrous membrane for photocatalysis and antimicrobial activity. *J. Colloid Interface Sci.* **2018**, *513*, 566–574. [[CrossRef](#)] [[PubMed](#)]
46. Iatsunskyi, I.; Vasylenko, A.; Viter, R.; Kempinski, M.; Nowaczyk, G.; Jurga, S.; Bechelany, M. Tailoring of the electronic properties of ZnO-polyacrylonitrile nanofibers: Experiment and theory. *Appl. Surf. Sci.* **2017**, *411*, 494–501. [[CrossRef](#)]
47. Tereshchenko, A.; Smyntyna, V.; Ramanavicius, A. Interaction mechanism between TiO<sub>2</sub> nanostructures and bovine leukemia virus proteins in photoluminescence-based immunosensors. *RSC Adv.* **2018**, *8*, 37740–37748. [[CrossRef](#)] [[PubMed](#)]
48. Viter, R.; Jekabsons, K.; Kalnina, Z.; Poletaev, N.; Hsu, S.H.; Riekstina, U. Bioanalytical system for detection of cancer cells with photoluminescent ZnO nanorods. *Nanotechnology* **2016**, *27*, 465101. [[CrossRef](#)] [[PubMed](#)]
49. Viter, R.; Khranovskyy, V.; Starodub, N. Application of Room Temperature Photoluminescence from ZnO Nano-rods for Salmonella Detection. *IEEE Sens. J.* **2014**, *14*, 2028–2034. [[CrossRef](#)]

**Disclaimer/Publisher's Note:** The statements, opinions and data contained in all publications are solely those of the individual author(s) and contributor(s) and not of MDPI and/or the editor(s). MDPI and/or the editor(s) disclaim responsibility for any injury to people or property resulting from any ideas, methods, instructions or products referred to in the content.